Saudi Pharmaceutical Journal 29 (2021) 223–235

Contents lists available at ScienceDirect

Saudi Pharmaceutical Journal

journal homepage: www.sciencedirect.com

Original article

Inclusion complex of clausenidin with hydroxypropyl-β-cyclodextrin: Improved physicochemical properties and anti-colon cancer activity

Ashwaq Shakir Al-Abboodi [a,*], Warqa'a Muhammed Al-Sheikh [a], Eltayeb E.M. Eid [b], Faizul Azam [b], Mothanna Sadiq Al-Qubaisi [c]

[a] Basic Science Branch, Faculty of Dentistry, University of Al-Qadisiyah, Al-Diwaniyah, Iraq
[b] Depratemnt of Pharmaceutical Chemistry and Pharmacognosy, Unaizah College of Pharmacy, Qassim University, Saudi Arabia
[c] Institute of Bioscience, Universiti Putra Malaysia, 43400 UPM Serdang, Selangor, Malaysia

ARTICLE INFO

Article history:
Received 22 July 2020
Accepted 20 January 2021
Available online 3 February 2021

Keywords:
Clausenidin
Hydroxypropyl-β-cyclodextrin
Drug release
Physicochemical characterization
Cell cycle
Reactive oxygen species

ABSTRACT

The long-term objective of the present study was to prepare, physicochemically characterize and determine the anticancer of clausenidin/hydroxypropyl-β-cyclodextrin (Clu/HPβCD) inclusion complex. We used differential scanning calorimetry, X-ray diffractometer, fourier transform infrared spectroscopy, ultraviolet–visible spectrophotometer and ^{13}C and ^{1}H nuclear magnetic resonance followed by *in vitro* anticancer assays. The orientation and intermolecular interactions of Clausenidin within cyclodextrin cavity were also ascertained by molecular docking simulation accomplished by AutoDock Vina. The guest molecule was welcomed by the hydrophobic cavity of the host molecule and sustained by hydrogen bond between host/guest molecules. The constant drug release with time, and increased solubility were found after successful complexation with HPβCD as confirmed by physicochemical characterizations. Clausenidin had greater cytotoxic effect on colon cancer HT29 cells when incorporated into HPβCD cavity than dissolved in DMSO. Also, from a comparison of cell viability between normal and cancer cells, a reduced side effect was observed. The Clu/HPβCD inclusion complex triggered reactive oxygen species-mediated cytotoxicity in HT29 cells. The inclusion complex-treated HT29 cells showed cell cycle arrest and death by apoptosis associated with caspases activation. The presence of HPβCD seems to aid the anticancer activity of clausenidin.

1. Introduction

Pyranocoumarins are a group of naturally occurring organic compounds, secondary metabolites, and are widely distributed in the plant kingdom. They are regularly consumed by humans, as they are common constituents of fruits, vegetables and teas (Ramawat and Mérillon, 2013). Clausenidin is a yellow-colored pyranocoumarin compound, isolated from *Clausena excavata*, (Joshi et al., 1967). Clausenidin has a variety of pharmacological properties, including antioxidant (Damsud et al., 2017), antidiabetic (Damsud et al., 2017), anti-inflammatory (Brezani et al., 2018), antibacterial (Sunthitikawinsakul et al., 2003), antiviral (Kongkathip et al., 2005; Su et al., 2009), antifungal (Sunthitikawinsakul et al., 2003), and anticancer activities (Waziri et al., 2018). Due to this range of pharmacological activities, this compound has been standing out, making its use increasingly attractive and sought after (Srivastava and Pandey, 2015).

Regarding the anti-cancer capacity, the effect of clausenidin against several different types of malignant neoplasms was studied by Waziri et al. (2018) reported that clausenidin inhibits the *in vitro* growth of cancer cells from human with hepatocellular carcinoma (Waziri et al., 2018). The antioxidant capacity of clausenidin could be implicated in the prevention of carcinogenesis, especially when induced by chemicals (Arbab et al., 2011; Damsud et al., 2017). This potential has led to numerous *in vitro* and *in vivo* studies that have provided ample evidence that clausenidin can prevent carcinogenesis and inhibit tumor origin through different molecular mechanisms (Waziri et al., 2018).

However, clausenidin and related coumarins have a relatively low oral bioavailability due to its low aqueous solubility

* Corresponding author.
E-mail address: ashwaq.shaker@qu.edu.iq (A.S. Al-Abboodi).

Peer review under responsibility of King Saud University.

Production and hosting by Elsevier

https://doi.org/10.1016/j.jsps.2021.01.006
1319-0164/

(Bourgaud et al., 1994), which limits its application in the clinic. Thus, it appears that for the development of a solid formulation containing clausenidin, the use of adjuvants or other pharmacotechnical strategies that promote increased solubility and oral absorption must be combined.

The oral route, among the routes used for the administration of drugs, stands out for its advantages such as greater acceptance by the patient, safety, possibility of presenting a systemic effect and low cost (Florence and Salole, 2013).

However, the development of solid oral dosage forms requires care and involves many steps, including a preformulation study. This in turn covers a study of drug-excipient compatibility to obtain a suitable final product, since the incompatibility between drug and excipients can change the stability and bioavailability of drugs, and thus affect their safety and effectiveness (Arcangelo and Peterson, 2006; Florence and Salole, 2013). Nevertheless, some interactions are planned with the objective of increasing the solubility and/or bioavailability of the drug, such as the drug-cyclodextrin complexation or the formulation of solid dispersions (Saokham et al., 2018).

The use of cyclodextrins (CD), which are cyclic oligosaccharides obtained from the intramolecular transglycolation of starch, presents itself as an alternative to improve the solubility of molecules (Praphanwittaya et al., 2020). This is attributed to its conical spatial structure with the orientation of hydroxy groups to the outside confer unique physical–chemical properties, being capable of being solubilized in aqueous medium and at the same time encapsulating hydrophobic molecules inside its cavity (Gratieri et al., 2020).

The use of cyclodextrin as a strategy to increase the solubility of dentatin (isolated from *Clausena excavata*) has already been described in our previous work (Ashwaq et al., 2017), and different methods have been used to prepare and characterize its complexes.

However, it is important to point out that, to date, no studies have been published to characterize the clausenidin: CD complexes using calorimetric, spectroscopic and microscopic techniques. In view of the above, clausenidin/hydroxypropyl-beta-cyclodextrin (Clu/HPβCD) complex was developed, characterized and their anti-cancer properties determined *in vitro*.

2. Materials and methods

2.1. Chemicals and reagents

Clausena excavata Burm. F. used in this study was collected from Pendang, Kedah, Malaysia. The clausenidin was extracted and purified, then subjected to glass column chromatography through silica gel to obtain pure compound crystals as previously reported (Waziri et al., 2016). The electron impact-mass spectrum (EI-MS) analysis indicates that the compound in the purified extract was clausenidin (Fig. 1). Hydroxypropyl-beta-cyclodextrin (HPβCD) (MW 1396) was purchased from sigma Aldrich (St. Louis, MO, USA). Average degree of substitution in HPβCD is 0.67 hydroxypropyl groups per glucose unit. Trypsin/ethylenediaminetetrace tic acid (EDTA) solution was purchased from Invitrogen (Carlsbad CA, USA). Dimethyl sulfoxide (DMSO), phosphate-buffered saline (PBS), 3-(4,5-dimethylthiazol-2-yl)-2,5-diphenyltetrazolium bromide (MTT), Dulbecco's modified Eagle's medium (DMEM), and trypan blue dye were purchased from Sigma Chemical Company (Perth, WA, Australia).

2.2. Preparation of clausenidin/hydroxypropyl-beta-cyclodextrin complex

The clausenidin/hydroxypropyl-beta-cyclodextrin (Clu/HPβCD) complex was prepared using the mixing method as described previously (Al-Qubaisi et al., 2019). Clausenidin (0.3284 mg), and HPβCD (1.396 mg) were dispersed in 2.5 mL of water, in completely closed amber glass bottles. The molar ratio in dispersions was 1:1. The aqueous dispersion was subjected to agitation in a 37 °C water bath for 48 h. After this period, they were cooled to 25 °C and filtered through 0.45 μm filter membranes into 5.0 mL volumetric flasks. One litre of aqueous dispersions was produced. Powdered Clu/HPβCD complex was produced by freeze drying the aqueous solution. Drying was carried out under − 60 °C and 0.2 torr. The physical mixture of clausenidin and hydroxypropyl-beta-cyclodextrin in the same weight ratio as the dried complex was prepared. The clausenidin and HPβCD were admixed in a mortar and pestle for 5 min to obtain a homogenous powder.

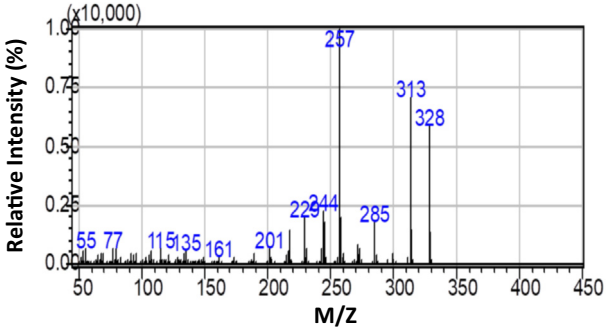

Fig. 1. Electron impact mass spectrum (70 eV) of extracted clausenidin.

2.2.1. Drug content and encapsulation efficiency

The total amount of free or unincorporated drug was determined using UV–Vis spectrophotometer (Model Perkin Elmer Lambda 35) at λ_{max} = 280 nm. Calibration curve for clausenidin was prepared in the concentration range of 0.0–100.0 μg/ml at corresponding wavelength. To calculate drug loading, the amount of drug incorporated in the complex was determined after subtracting unincorporated drug amount from total known amount of added drug. Encapsulation efficiency is equal to amount of incorporated drug divided by complex amount.

2.2.2. Drug release

The drug release profile is very important in the design of a release system, since understanding the release process helps to determine its mechanism, in order to improve the release kinetics. In the normal differentiated adult cells, the intracellular pH is generally ~7.2 and lower than the extracellular pH of ~7.4 (Cao et al., 2019). The evaluation of the *in vitro* release of the clausenidin incorporated in HPβCD, was performed using the spectrophotometer technique in the ultraviolet–visible (UV–Vis) region. Using same methods, reported in our previous work (Al-Qubaisi et al., 2019), it is possible to determine the absorbance, concentration, mass released and fraction released of the drug in relation to each tested concentration. The *in vitro* release of the drug was studied in phosphate buffer solution PBS (pH 7.4). The release medium was quantified by direct measurement of absorbance at 280 nm, performed on UV–Vis spectrophotometer (Model Perkin Elmer Lambda 35). To analyze the profile of drug release from inclusion complex, software KinetDS 3.0 (Mendyk et al., 2012) was used. The results of drug release were fitted to kinetic models of zero-order (1) and first-order (2), second-order (3), Higuchi (4), KorsmeyerPeppas (5), Weibull (6), Hixson-Crowell (7), Michaelis–Menten (8) and Hill (9). The best-fit determines the model that best described the drug release curve, mainly by the Empirical R^2 R^2_{emp} (14), Akaike information criterion AIK (15), Bayesian information criterion Schwarz criterion BIC (16) and Root-mean-squared

error RMSE (17). The dissolution efficiency DE% (10) and mean dissolution time MDT (11) have been also computed by KinetDS 3.0 software (Patel et al., 2008).

$$Q = k.t + Q_0 \quad (1)$$

$$\frac{1}{Q} = k.t + \frac{1}{Q_0} \quad (2)$$

$$\frac{1}{Q^2} = k.t + \frac{1}{Q_0^2} \quad (3)$$

$$Q = k.\sqrt{t} \quad (4)$$

$$Q = k.t^n \quad (5)$$

$$Q = 100.\left[1 - exp\left(\frac{-(t - T_{LAG})^b}{a}\right)\right] \quad (6)$$

$$Q^{\frac{1}{3}} = k.(t - T_{LAG}) + Q_0^{\frac{1}{3}} \quad (7)$$

$$Q = \frac{Q_{max}.t}{k + t} \quad (8)$$

$$Q = \frac{Q_{max}.t^n}{k^n + t^n} \quad (9)$$

$$DE = \frac{\int_0^t Qdt}{Q_{max}.t} * 100 \quad (10)$$

$$MTD = \frac{\sum_{j=1}^{n} t_j^{AV} * \Delta Q_j}{\sum_{j=1}^{n} \Delta Q_j} \quad (11)$$

$$\Delta Q = Q_{(t)} - Q_{(t-1)} \quad (12)$$

$$t_j^{AV} = (t_i + t_{i-1})/2 \quad (13)$$

$$R_{emp}^2 = 1 - \frac{\sum_{i=1}^{N} (y_i - \hat{y}_i)^2}{\sum_{i=1}^{N} (y_i - y_{AV})^2} \quad (14)$$

$$AIC = 2k + N.\left[In\left(\sum_{i=1}^{N} (y_i - \hat{y}_i)^2\right)\right] \quad (15)$$

$$BIC = N.In\left(\sum_{i=1}^{N} (y_i - \hat{y}_i)^2\right) + k.In(N) \quad (16)$$

$$RMSE = \sqrt{\frac{\left(\sum_{i=1}^{N} (y_i - \hat{y}_i)^2\right)}{N}} \quad (17)$$

Q: amount (%) of drug substance released at the time t Q_0: start value of Q Q_{max}: maximum value of Q (100%) T: time k, a, b: constants T_{LAG}: lag time y_i: observed value $\hat{y}_i$: model-predicted value y_{AV}: average output value (Patel et al., 2008).

2.2.3. Phase solubility

To determine the solubility of clausenidin in the acceptor medium, the excess solubility method was performed. Clausenidin, in excess, and hydroxypropyl-β-cyclodextrin in different concentrations, were dispersed in 2.5 mL of water, in closed amber glass bottles. The aqueous dispersions were subjected to agitation in a 37 °C water bath for 48 h. After this period, they were cooled to 25 °C and filtered through 0.45-μm filter membranes into 5.0 mL volumetric flasks. A 1.0 mL aliquot of each filtrate was removed and diluted in chloroform, to a volume of 3.0 mL for analysis with λ_{max} = 280 nm using UV–Vis spectrophotometer (Model Perkin Elmer Lambda 35).

2.3. Physicochemical properties of Clu/HPβCD complex

2.3.1. Scanning electron microscopy

Scanning electron microscopy (SEM, Model LEO 1450VP [LEO Electron Microscopy Ltd Cambridge, UK]) was used to determine the morphology of clausenidin, HPβCD, physical mixture and Clu/HPβCD inclusion complex. The samples were degassed in an evacuated heated chamber at 100 °C overnight. Prior to SEM scanning, dried samples were spread over double-sided conductive tape adhered to the specimen stub.

2.3.2. X-ray diffraction

The diffractograms of clausenidin, HPβCD, physical mixture and inclusion complex were recorded using a Shimadzu XRD-6000 instrument (Shimadzu Corporation, Kyoto, Japan) under the following operating conditions: CuKα radiation (l = 1.5406 Å), voltage of 30 kV, current of 30 mA, scanning rate of 0.5° 2θ.min^{-1} in the range of 5°–37° and at room temperature (22.5 °C).

2.3.3. Fourier transform infrared

The infrared spectrum was obtained by gently mixing samples with potassium bromide agate (Al-Qubaisi et al., 2013b). Both raw materials (clausenidin and HβCD), physical mixture and inclusion complex were analyzed on a Thermo Nicolet Nexus, Smart Orbit spectrometer.

2.3.4. Differential scanning calorimetry (DSC)

The analyses were carried out in a differential calorimeter (DSC Model Mettler Toledo 821e) by heat flow, equipped with a flow controller for purge gas (N_2). In order to carry out the test, approximately 1.0 mg of the clausenidin, HPβCD, physical mixture and inclusion complex were transferred to an aluminum sample holder, which was sealed and placed in the oven. The heating ramp used was 10 °C/min to 280 °C and the nitrogen flow was 50 mL/minute.

2.3.5. ^{13}C and ^{1}h nuclear magnetic resonance (NMR)

Both ^{13}C and ^{1}H NMR experiments have been performed in deuterated DMSO on Bruker with cryoprobe (700 MH_z) (USA)spectrometer at 298 K. Chemical shifts are given in ppm relative to tetramethylsilane as an internal standard (δ = 0).

2.3.6. Molecular docking

AutoDock Vina 1.1.2 (Trott and Olson, 2010) was utilized in current study to predict the most likely optimal configuration of the Clu/HPβCD inclusion complex. The three-dimensional structure of β-cyclodextrin was retrieved from the Protein Data Bank (PDB ID: 1z0n) and modified by adding seven hydroxypropyl moieties using ChemBio3D Ultra 12.0 (CambridgeSoft, Cambridge, MA, USA) program. Chemical structure of clausenidin was obtained from PubChem database in sdf format. Both HPβCD and clausenidin molecules were then optimized by PM3 semi empirical energy minimization protocol implemented in ChemBio3D Ultra 12.0 and saved in pdb format. MGLTools 1.5.6. was used for merging all nonpolar hydrogen and adding gasteiger charges to all atoms of the optimized HPβCD and clausenidin molecules. The resolution of grid was 16 × 16 × 16 points, with a grid spacing of 1 Å and positioned at −7.17, 37.44 and −6.74 in ×, y and z directions, respectively. AutoDock Vina 1.1.2 was used for molecular docking using default parameters considering flexible clausenidin and rigid HPβCD. At the end of the docking, top ten conformations were individually

visualized in Biovia Discovery Studio Visualizer 2020 and Chimera programs.

2.4. Cell culture

Two human cell lines, colorectal adenocarcinoma (HT29) and normal colon (CCD-18Co) were obtained from the American Type Culture Collection (ATCC; Rockville, MD, USA). The cells were cultured in DMEM (Sigma Aldrich, USA) supplemented with 10% FBS and 1% penicillin (100 U/mL) (Isocillin, Aventis, Germany) in an incubator at 37 °C in the presence of 5% CO_2.

2.5. 3-(4,5-dimethylthiazol-2-yl)-2,5-diphenyltetrazolium bromide assay

The Clu/HPβCD complex was mixed well in DMEM medium (Sigma Aldrich, USA) containing fresh 10% heat-inactivated FBS and colloidal suspension was obtained using ultrasound method (Al-Qubaisi et al., 2013b). Clausenidin was dissolved in DMSO. Two hundred microliters of 5×10^4 cells/mL suspension were added to each well of a 96-well cell culture plate at a final concentration of 1×10^4 cells/well. The media was aspirated and replaced with 200 µL fresh media containing compound of concentrations ranging from 0.2969 to 19 µg/mL dissolved in DMSO or complexed with HPβCD. The last row was used for the nontreated control. The plate was then incubated at 37 °C under 5% CO_2, for 24 h. The medium was aspirated and the cells washed with PBS trice to remove the test compounds, and fresh medium added. The medium was aspirated after two hours and 200 µL medium containing 5 mg/mL 3-(4,5-dimethylthiazol-2-yl)-2,5-diphenyltetrazolium bromide (MTT) solution were added to each well and the plate incubated for 4 to 6 h at 37 °C under 5% CO_2. The MTT-containing medium was then carefully removed and replaced with 200 µL DMSO/well, to dissolve the formazan crystals. The plate was read on automated spectrophotometric EL 340 multiplate reader (Bio-Tek Instruments Inc., USA) at 570 nm. The viability percentage is calculated by:

$$(OD_{\text{treated well}})/(OD_{\text{nontreated well}}) \times 100 \quad (18)$$

OD refers to optical density

For each test compound and cell line, the 24 h IC_{50} values (50% cell growth inhibition concentration) were determined from the dose–response curves.

2.6. Caspase-3 and -9

The enzyme activities of both caspases were examined using a colorimetric protease assay kit (ApoTarget, Camarillo, CA). Cells were seeded at 6×10^6 cells total, rested for 4 h, and incubated in 37 °C 5% CO_2 for 24 h in 2 mL media containing clausenidin (either dissolved in DMSO or complexed with HPβCD) at IC_{50} concentrations. Cells were pelleted and then re-suspended in Cell Lysis Buffer (ApoTarget) before being microcentrifuged. The supernatant containing the protein from lysed cells was transferred to a fresh tube on ice. The protein concentration was assayed by bicinchoninic acid (BCA) assay, in which, different protein concentrations were diluted to standardize total protein content. Reaction buffer, dithiothreitol (DTT), and DEVD-pNA or LEHD-pNA substrates (ApoTarget) were added and the plate incubated in 37 °C 5% CO_2 and measured using microplate reader at 405 nm.

2.7. Microscopic examination of cell morphology

After culturing HT29 cells in a 6-well tissue culture plate at (1×10^5 cells/well) for 24 h, cells were then treated with clausenidin, dissolved in the DMSO or incorporated into HPβCD, corresponding to IC_{50} values obtained from MTT results, as well as cells devoid of any treatment (negative control). Cellular morphological changes were then observed at 24 h using phase contrast microscope at 200X magnification.

2.8. Morphological assessment of apoptotic cells by acridine orange (AO) propidium iodide (PI) double staining

HT29 cells were treated with clausenidin, dissolved in the DMSO or incorporated into HPβCD, corresponding to IC_{50} values obtained from MTT results. The medium with the detached cells were then pipetted off, centrifuged and pooled with the adherent cells then pelleted at 1700 rpm for 5 min. The cell pellet was then washed once with PBS and resuspended in new PBS at a final concentration of 10^6 cells/mL. For staining, 2 µL of the AO/PI solution were added to 50 µL of cell suspension, mixed thoroughly and incubated at room temperature for 5 min in the dark. The stained cells were then applied to a slide, covered with a cover slip and counted under a fluorescence microscope (Olympus, Japan) at an excitation wavelength of 490 nm.

2.9. Cell cycle assay

The HT29 cells were collected after treated with clausenidin at IC_{50} concentrations (8.22 µg/mL dissolved in the DMSO or 2.42 µg/mL incorporated into HPβCD) for 24 h. Cells were washed two times with cold PBS, re-suspended in 200 µL PBS and fixed in 2 mL of ice-cold 70% ethanol for two hours at 4 °C. The fixed cells were stored at 4 ^{0}C until analysis. Prior to analysis, the fixed cells were centrifuged then resuspended in PBS. Then the cells were stained with a propidium iodide solution (50 µg/ml) containing RNase A (0.1 mg/ml) in PBS at 37 ^{0}C for 15 min. After mechanical dispersion of stained cells using a 25-gauge syringe needle, cell cycle analyses were carried out by flow cytometery (FACS, Beckman Coulter). For each condition, the cell cycle distribution of at least 10,000 cells was analyzed. The number of cells in G_1/G_o, S and G_2/M phases was calculated from the resultant DNA histogram. Cells in the sub-G1 peak of the DNA histogram represented those containing a sub-diploid amount of DNA and were regarded as apoptotic.

2.10. Reactive oxygen species

CM-H_2DCFDA (5- (6) -chloromethyl-2 ', 7′-dichlorodihydrofluor escein diacetate, acetyl ester) is a cell-permeable compound and is applied to determine the amount of intracellular reactive oxygen species (ROS) (LaManna et al., 2011). Human colon cancer HT29 cells ($1.0x10^6$ cells) were grown in 25 cm^2 flask and incubated to allow them to attached on the flask wall for 24 h at 37 °C and 5% CO_2. After this period, the medium was removed and the cells were treated only with DMEM culture medium (control group) or treated with clausenidin complexed with HPβCD or clausenidin dissolved in DMSO at IC_{50} concentrationsfor 24 h at 37 °C and 5% CO_2. Then, the medium was removed and the cells were incubated with 1 mL of the CM-H_2DCFDA solution for 30 min. After this incubation period, the dye solution was removed, the cells were harvested from the flask and centrifuged at 500 × g for 5 min at 4 °C. Finally, the cells were washed twice with PBS, placed on ice and covered to protect them from light. The samples were analyzed by flow cytometry (FACS, Beckman Coulter).

2.11. Statistical analysis

All experiments were done in triplicates. Data were expressed as mean ± standard deviation. All statistical analyses were performed using Minitab statistical software (Minitab Inc., State College, PA). Treatment effects were determined using one-way

analysis of variance (ANOVA) followed by Tukey's post-hoc analysis. A value of $p < 0.05$ was considered significant unless otherwise indicated.

3. Results

3.1. Material characterization

3.1.1. Scanning electron microscopy

Fig. 2.A illustrated the surface morphology of HPβCD, clausenidin, physical mixture and inclusion complex under SEM magnification. HPβCD was observed to be spherical and porous irregular in shape (Fig. 2.A.4), while clausenidin presented long strips (Fig. 2.A.1). The physical mixture was seen as a combination of the morphology of the clausenidin and HPβCD (Fig. 2.A.3). In the case of inclusion complex, the original morphology of both the parent components had disappeared (Fig. 2.A.2). These changes suggested the successful formation of inclusion complex. Moreover, the inclusion complex showed a non-uniform particle size distribution with an aggregation, and there was no gap between the particles, thus suggesting poor redispersibility.

3.1.2. Differential scanning calorimetry (DSC)

Fig. 2.B shows the thermograms of clausenidin, HPβCD, physical mixture and inclusion complex. Clausenidin showed one endothermic peak at 137 °C, consistent with its melting point and its crystalline nature. The melting point provided by the DSC equipment is called the onset melting temperature (T_{onset}), the temperature at which the extrapolated baseline intersects with the leading edge of the extrapolated transition temperature. This temperature is not influenced by the heating speed (Earnest and Measurements, 1988; Clausse and Dumas, 2016). Similar to our previous study (Al-Qubaisi et al., 2019), the HPβCD showed a peak at 69 °C which correspond to glass transition (Tg). The thermogram of the physical mixture (clausenidin with HPβCD at 1:1 ratio) showed two endothermic peaks which corresponded to clausenidin and HPβCD. On the other hand, the peak around 137 °C was enormously disappeared compared to that of pure clausenidin, indicating successful formation of the inclusion complex.

3.1.3. X-ray diffraction

The X-ray diffractograms of the clausenidin, HPβCD, physical mixture and inclusion complex are shown in Fig. 2.C. The peaks related to clausenidin are located at values 2θ = 8.64; 9.97; 10.92 and 12.47°. The intense peaks of clausenidin indicate its presence in large crystalline grains. The diffractogram clearly shows the characteristic peak of clausenidin, the forth being intense peaks, making it possible to calculate the crystallite size through the Scherrer Equation (Al-Qubaisi et al., 2013b). The value for the peak at 2θ = 12.47 °C orrespond to a crystallite size of 104.2 Å. The appearance of an intense peak at 12.3° after the physical mixing of clausenidin with HPβCD is attributed to nonsuccessful incorpo-

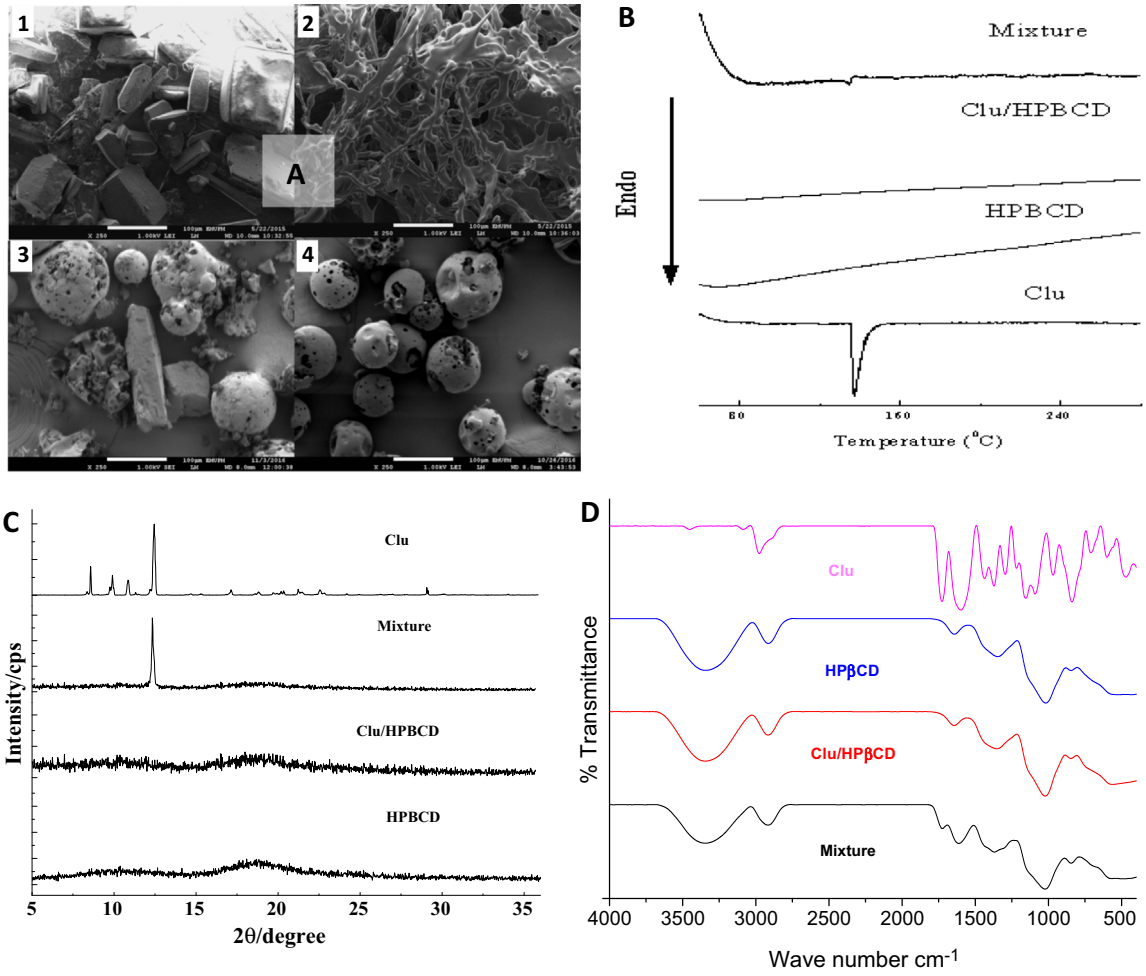

Fig. 2. Characterization of clausenidin (Clu), hydroxypropyl-beta-cyclodextrin (HPβCD), physical mixture and clausenidin/hydroxypropyl-beta-cyclodextrin (Clu/HPβCD) complex by: **A)** SEM micrographs of Clu (1), Clu/HPβCD (2), physical mixture (3) and HPβCD (4). B) Differential scanning calorimetric curves for the samples C) X-ray diffraction (XRD) pattern of the samples. D) Fourier transform infrared spectrum of samples.

ration of compound into cyclodextrin cavity. No crystal phase was observed in both diffractograms of HPβCD and inclusion complex. Similar to HPβCD, the powdered inclusion complex presented two halos in the region of 2θ between 7 and 22.5°, characteristic of amorphous solids, with no peaks related to clausenidin, indicating full incorporation of compound into cyclodextrin hydrophobic cavity.

3.1.4. Infrared absorption bands

The infrared spectra of clausenidin and HPβCD are shown in Fig. 2.D. The spectrum of clausenidin is observed, where a characteristic band of phenolic hydroxyl can be observed in the region between 4000 and 3000 cm $^{-1}$ (3450 cm $^{-1}$) and another band of aromatic ring (3092 cm $^{-1}$). A 1728 cm^{-1} signal, corresponding to the C=O stretching regions, and another signal around 1605 cm^{-1}, which suggests the presence of aromatic C=C stretching, are also observed. Peaks at 1440 cm^{-1} and 1371 cm^{-1} were also measured, which could be reconciled with the C—H stretching of methyl groups. Methoxy C—O, phenolic C—O, C—O of the ester group and C—O of the aryl ester group were responsible for the formation of the peaks at 1294 cm^{-1}, 1221 cm^{-1}, 1161 cm^{-1}, and 1086 cm^{-1}, respectively.

The spectrum of the HPβCD presents a broad band between 3700 and 3050 cm^{-1} and a band in the region of 2920 cm^{-1}, which characterizes a C—H stretch proper to sugars. The complex group of bands between 1221 and 890 cm^{-1} characterize the C—O stretch of ether and OH, respectively. The double band around 846 cm^{-1} is also a characteristic band for sugars.

Fig. 2.D represents the dried complex infrared spectrum and the simple mixture. As can be seen, the broadband of the HPβCD overlap with the characteristic bands of clausenidin in this same region (3800–2900 cm^{-1}). This observation is expected, since the mass of the pyranocoumarin present, both in the simple mixture and in the complex, is quite small when compared to the mass of cyclodextrin in both samples (MW of clausenidin = 328, MW of HPβCD = 1396). Bands of clausenidin are quite attenuated due to the reduced amount of pyranocoumarin in the complex and correspond to ring C of clausenidin. Both, complex and simple mixture, contain the same amount of clausenidin.

3.1.5. Phase solubility

The realization of the solubility diagram is of great importance to verify the effect of the association of bioactive substances with cyclodextrins, on their solubility, considering the possibility of formation of inclusion complexes. Through the determination of clausenidin in the solution submitted to complexing conditions in liquid medium, an increase in solubility for the compound under study was verified Fig. 3.A. Adding HPβCD (at 1 mM) leads to increase sloubility of clausenidin from 0.045 to 2.56 mM. Thus, the solubility increased up to 56 times in relation to clausenidin in water (without the presence of HPβCD). The curve found was of A_L-type, which characterizes a linear relationship (R^2 > 0.96) between the increase in solubility of clausenidin and the concentration of cyclodextrin. Non-linearity of solubilisation can be rationalised by two contributions: cyclodextrin–drug interaction and the drug-induced change of cyclodextrin – cyclodextrin interaction (Nicol et al., 2016).

The graphical representation of the solubility diagram can be seen in Fig. 3.A. The elaboration of the solubility diagram also allows the calculation of the apparent stability constant of the complex (K_c). This stability constant allows to classify the complex formed as labile or stable. It is calculated according to the equation presented below, described by (Al-Qubaisi et al., 2019).

$$K_c = \frac{S_t - S_0}{S_0(L_t - S_t + S_0)}$$

where S_t is the total molar concentration of the compound in solution; S_0 is the molar concentration of compound S in the absence of cyclodextrin (L); L_t is the total molar concentration of cyclodextrin.

In the experimental conditions presented, the apparent stability constant K_c calculated for the clausenidin: cyclodextrin complex was 142.019 M^{-1}, therefore, it is considered a stable complex. This data shows that clausenidin is not capable of leaving the cavity with ease. In the case of the experiment carried out in this work, the amount of cyclodextrin at the last point of the curve (10 mM) could be increased in order to obtain a greater increase in solubility of the clausenidin, however the saturation concentration of the aqueous medium with drug can also influence this solubility limit (Al-Qubaisi et al., 2019).

3.1.6. Drug content and release

The drug content and encapsulation efficiency of clausenidin in the inclusion complex were approximately 19.0 and 99.9%, respectively. The percentage of clausenidin released ranged from 3.4 to 29.4% after one and twelve hours, respectively. Fig. 3.B showed sustained release for more than five days from complex while clausenidin is rapidly released from the physical mixture and release is complete within 19 min at pH 7.4.

The results of drug release were fitted to different kinetic models as seen in Fig. 4. The readings were fitted to nine models

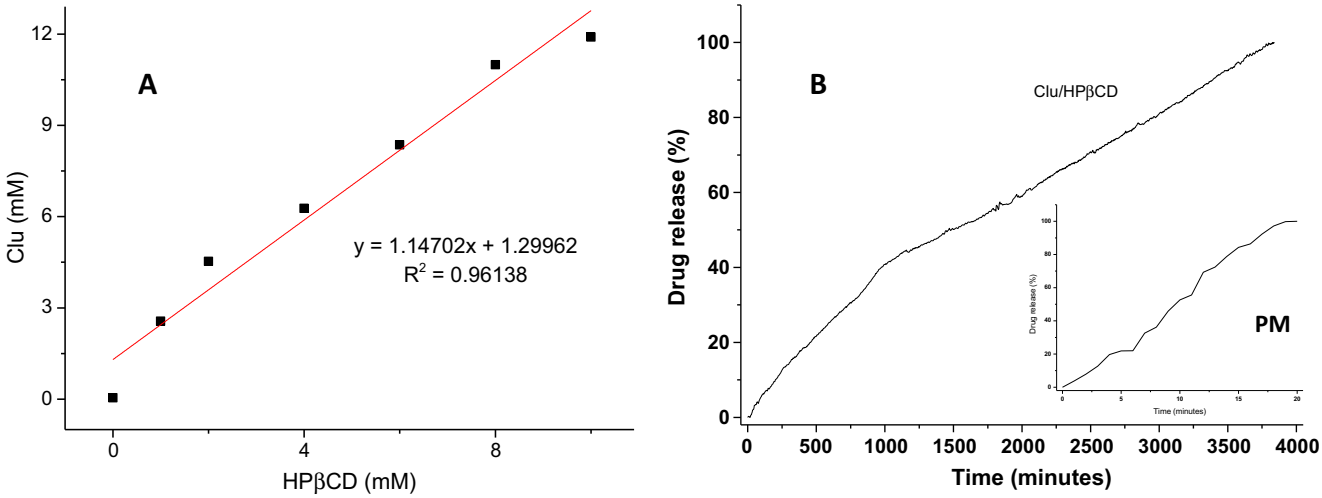

Fig. 3. Phase solubility (A) and drug release (B) of clausenidin (Clu) in the presence of hydroxypropyl-β-cyclodextrin (HPβCD).

describing drug dissolution. The AIK, BIC, R^2_{emp}, RSME values were the best for describing the release kinetics of clausenidin from the complex (Table 1). In phosphate buffer solution PBS (pH 7.4), the release profile of clausenidin did not follow the first-order, second-order, Hixson-Crowell, Michaelis-Menten, and Hill kinetics. The kinetic model that best described the dissolution curves for our formulation were the zero order model, with lowest reading observed at RMSE, AIC and BIC and highest reading observed at R^2_{emp}, and R^2 (Table 1).

3.1.7. Nuclear magnetic resonance

Nuclear Magnetic Resonance of protons (^{1}H NMR) and carbon (^{13}C –NMR) are a useful technique for characterizing the formation of inclusion complexes and it prove a useful experimental data on the nature of the interaction between the guest and host molecules. The chemical shifts of pure clausenidin and the inclusion complex indicate clear differences (Table 2). A remarkable upfield shift of H_9 and H_{10} protons of clausenidin in complex shows that the molecule penetrates the HPβCD cavity and it is stabilized by Van der Waals forces between the protons and the glycosidic oxygen of the HPβCD inner cavity (Table 2).

The same interactions were clearly seen in ^{13}C results (Table 3), in which C_9, C_8 and C_3 chemical shifts of clausenidin in the inclusion complex were changed by 2–5.5 ppm compared to the free clausenidin. This confirms the inclusion of clausenidin within the cavity of the cyclodextrin.

3.1.8. Molecular docking

The molecular docking results indicated that guest clausenidin could enter into the hydrophobic cavities of host HPβCD, possessing central alignment inside the molecule (Fig. 5). The central aromatic ring of the guest molecule carrying phenolic hydroxyl group participated in hydrogen bond interaction with the guest (HPβCD) molecule, stabilizing the docked clausenidin in the large hydrophobic cavity.

3.2. Anticancer of Pd/MgO nanoparticles

3.2.1. Cytotoxicity

The cytotoxicity of the clausenidin incorporated into HPβCD, the HPβCD, and the clausenidin dissolved in the DMSO was investigated. The cytotoxicity of clausenidin either dissolved in DMSO or complexed with HPβCD was insignificant ($p > 0.05$) on HT29 cancer cells at lowest concentration (0.29688 μg/mL) (Fig. 6). The clausenidin complexed with HPβCD exhibited a concentration-dependent cytotoxicity. At the concentration of 1.1875 μg/mL, the incorporated compound into HPβCD cavity significantly decreased ($p < 0.05$) viability of cancer cells by 40% while no notable change was observed in compound dissolved in DMSO.

At the concentration of 2.375 μg/mL, the cell viability of colon HT29 cancer cells was as high as 85% after treatment with clausenidin dissolved in DMSO, while approximately 50.3% of cells were only viable after exposure to compound complexed with HPβCD when compared to untreated cells. The inclusion complex with 2.42 μg/mL clausenidin concentration and 8.22 μg/mL of clausenidin dissolved in DMSO could be the IC_{50} concentration, in which the viability of HT29 cancer cells had reached its half value. The results obtained from MTT assay showed no significant change ($P > 0.05$) in the viability from normal colon CCD-18Co cells treated with inclusion complex at all concentrations for 24 h when compared to untreated cells. On the other hand, the CCD-18Co cells were sensitive to clausenidin dissolved in DMSO at concentrations of 9.5 and 19.0 μg/mL. HPβCD at all concentrations did not significantly ($P > 0.05$) inhibit growth of both cells.

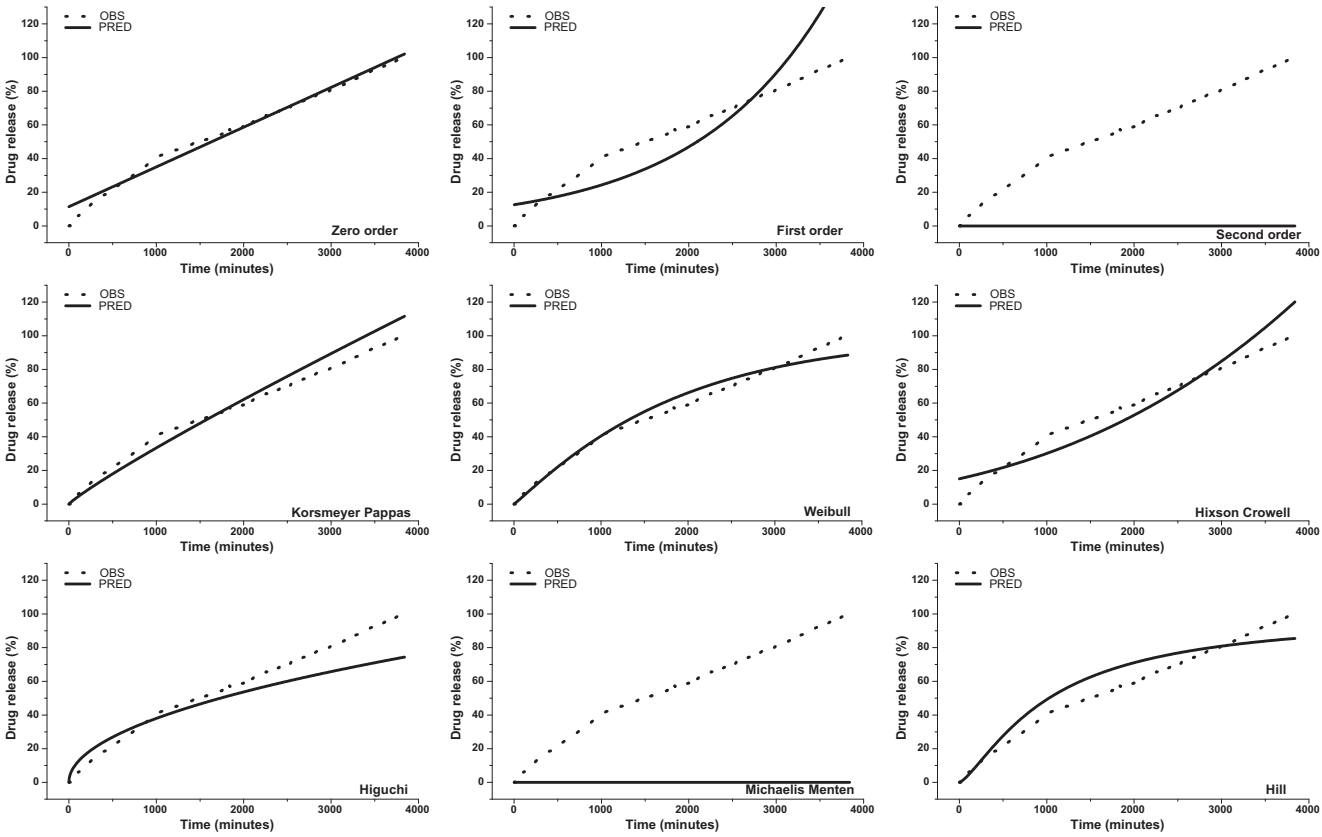

Fig. 4. Kinetic models of clausenidin release from clausenidin -loaded hydroxypropyl-β-cyclodextrin (Clu/HPβCD) in phosphate buffer solution PBS (pH 7.4). OBS and PRED are the observed and predicted values respectively.

Table 1
Data-fitting for clausenidin release from clausenidin -loaded hydroxypropyl-β-cyclodextrin (Clu/HPβCD) in phosphate buffer solution PBS (pH 7.4).

Model	Slope	Intercept	R^2	R^2_{emp}	RMSE	AIC	BIC	*k*
Zero-order	0.023633	11.390495	0.97081	0.98530	3.2027	12152.3	12162.6	–
First-order	0.000659	2.534267	0.08903	−3.96715	18.6755	16669.6	16679.9	–
Second-order	−24261.801930	62195462.267688	0.00002	−1387807544733.91990	62.6104	19768.9	19779.2	–
Korsmeyer-Peppas	0.897329	−2.691018	0.577100	−5311.72420	6.1839	13837.9	13848.2	0.068
Weibull	1.06384	−8.00729	0.64074	−7514.76132	4.5685	13062.2	13072.5	3002.777
Hixson-Crowell	0.000642	2.468205	0.70974	−3.98342	8.4591	14642.6	14658.0	0.001
Higuchi	0.500000	0.182904	0.65000	0.80623	11.6270	15455.5	15465.8	1.201
Michaelis-Menten	0.999219	7812500.062859	0.24961	−4.61895	62.6104	19770.9	19786.3	1.279E-07
Hill	1.343473	−9.313413	0.32203	0.89306	8.6374	14694.0	14704.3	11085.714
MTD	1659.972							
DE	56.7716							
No of timepoints	1281							

Table 2
^{1}H NMR chemical shifts ($^{\delta}$/ppm), chemical shifts variation (Δ^{δ}/ppm) and coupling constants (J/Hz) of clausenidin protons upon complexation with HPβCD.

Proton No.	Free δ_0	with HPβCD δ	Diff. in chem. Shifit $\delta - \delta_0$	Clausenidin Hz	Complex	J
H1	1.6	1.62	−0.02	640	648	−8
H2	5.25	5.2	0.05	2100	2080	20
H3	2.3	2.25	0.05	920	900	20
H4	2.3	2.22	0.08	920	888	32
H5	2.17	2.16	0.01	868	864	4
H6	2.17	2.16	0.01	868	864	4
H7	1.45	1.44	0.01	580	576	4
H9	1.8	0.95	0.85	720	380	340
H10	1.98	0.97	1.01	792	388	404
H11	1.12	1.07	0.05	448	428	20
H12	0.94	1.08	−0.14	376	432	−56
H13	5.75	4.79	0.96	2300	1916	384
H14	5.82	4.95	0.87	2328	1980	348
H15	4.67	4.59	−0.08	–	–	–
H16	3.99	3.02	−0.97	355	1650	−1295
H17	1.35	1.22	0.13	2100	810	−1290
H18	2.11	2.41	−0.3	405	577	−172
H19	2.01	2.34	0.33	2010	452	−1558
H20	2.84	2.78	−0.06	540	647	−107
H21	1.71	1.76	0.05	621	1020	−399
H22	2.51	2.59	0.08	712	1002	−290

Table 3
^{13}C NMR chemical shifts (δ/ppm), chemical shifts variation (Δ^{δ}/ppm) and coupling constant (J/Hz) clausenidin carbons upon complexation with HPβCD.

^{13}C	Free δ**0**	with HPβCD δ	Diff. in chem. Shift(Δδ) $\delta - \delta$**0**	Clausenidin Hz	Complex	J
C1	203.58	206.12	−2.54	81,432	82,448	−1016
C2	137.9	137.69	0.21	55,160	55,076	84
C3	148.94	151.1	−2.16	59,576	60,440	−864
C4	24.44	24.59	−0.15	9776	9836	−60
C5	40.46	40.31	0.15	16,184	16,124	60
C6	137.81	137.09	0.72	55,124	54,836	288
C7	125.06	125	0.06	50,024	50,000	24
C8	42.13	43.01	−0.88	16,852	17,204	−352
C9	38	43.22	−5.22	15,200	17,288	−2088
C10	160.76	163.12	−2.36	64,304	65,248	−944
C11	127.11	127	0.11	50,844	50,800	44
C12	12.13	12	0.13	4852	4800	52
C13	15.45	15	0.45	6180	6000	180
C14	29.31	30	−0.69	11,724	12,000	−276
C15						
C16						
C17						
C18						
C19						

3.2.2. Morphological examination

Human colon HT29 cancer cells possessed irregular surfaces appeared in clusters and clumps while cultures became less confluent when compared to untreated cells. Obvious characteristics of dead cells were observed at clausenidin, dissolved in the DMSO or incorporated into HPβCD, as the majority cells were detached (Fig. 7).

Untreated cells a green and normally structured cell nucleus and cytoplasmic area, while the treated cells exhibited dead cells at different apoptosis stages. Early apoptotic cells had a green, condensed,

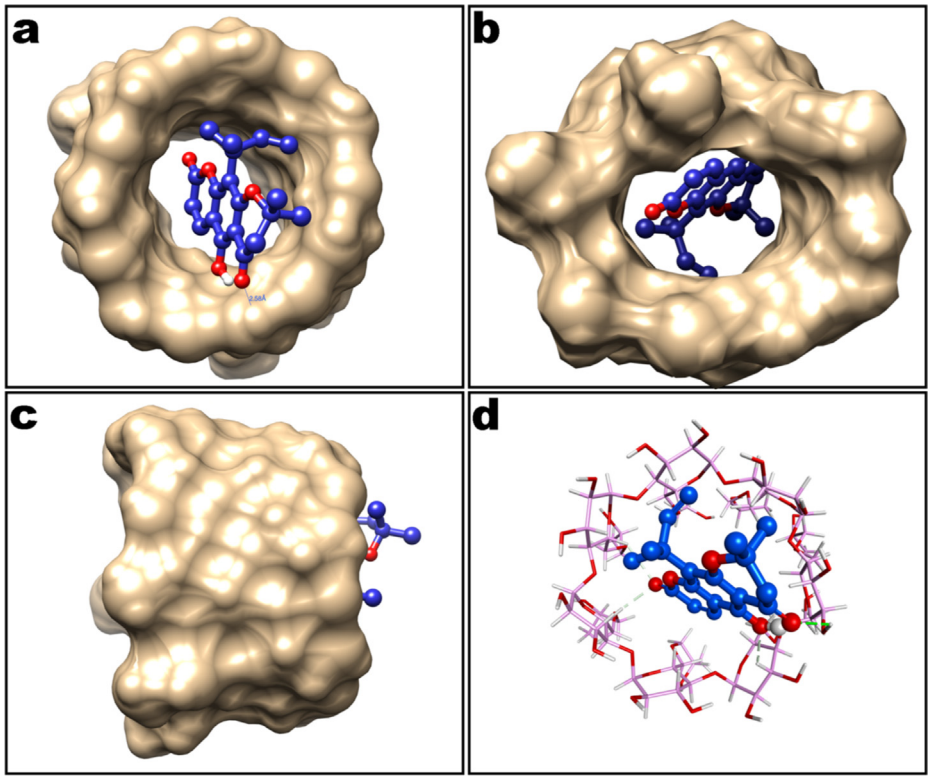

Fig. 5. Docking results of the inclusion complex formed between clausenidin(shown as ball and stick model in blue color) and hydroxypropyl β cyclodextrin (HPβCD, shown as surface rendering)(a) top view from the wide rim of HPβCD; (b) bottom view of HPβCD; and (c) side view of HPβCD; (d) HPβCD is represented as stick model, showing intermolecular interaction. Hydrogen bond is shown as green dotted line.

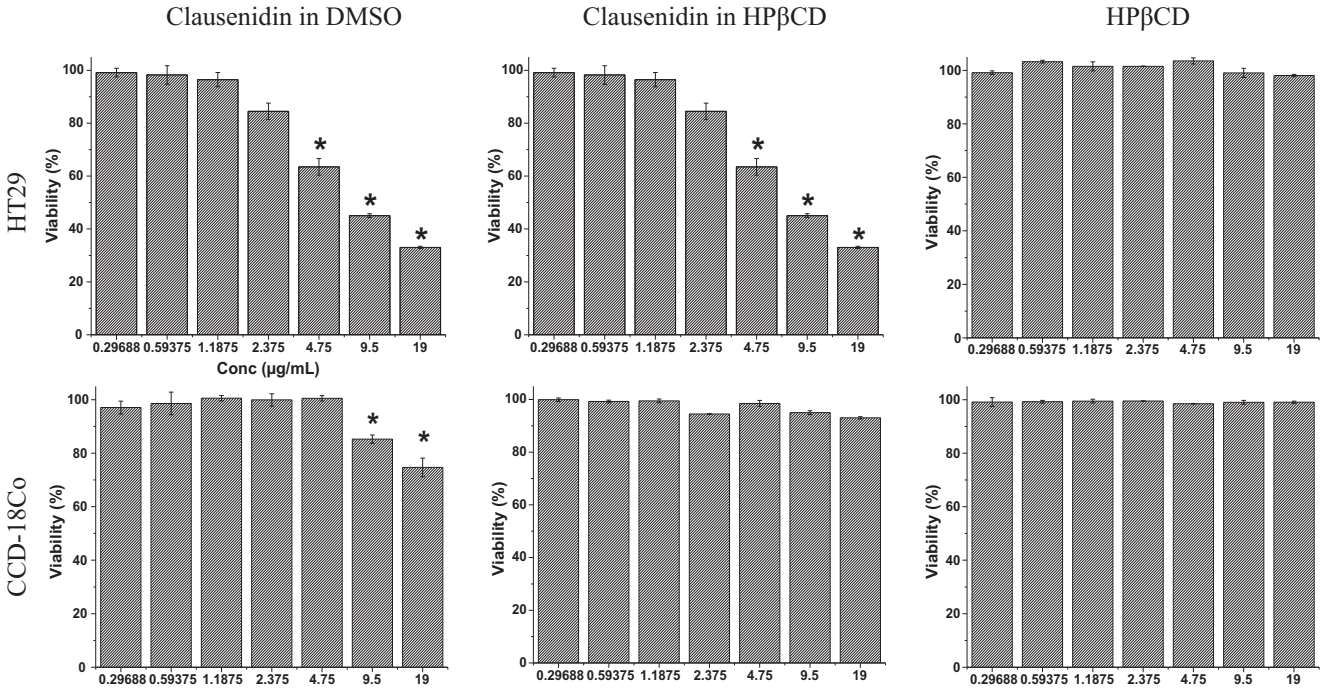

Fig. 6. Effects of clausenidin complexed with HPβCD or dissolved in DMSO, on the viability of treated cells, which were evaluated through mitochondrial activity using MTT assay. This assay was on colon cancer HT29 and normal colon CCD-18Co cells after 24 h. Mean ± standard deviation (n = 3 wells/treatment). *P < 0.05 compared to non-treated cells.

shrunk or fragmented cell nucleus while late apoptotic cells showed an red, condensed, shrunk or fragmented cell nucleus. Necrotic cells showed an orange, normally configured or ballooned cell nucleus (larger than normal). The clausenidin, dissolved in the DMSO or incorporated into HPβCD, corresponding to IC_{50}values, showed the typical features of classic apoptosis: shrunk cells and condensation of the cell nucleus. Some cell membranes remained intact (green color), and only at a later stage lost the integrity of the cell mem-

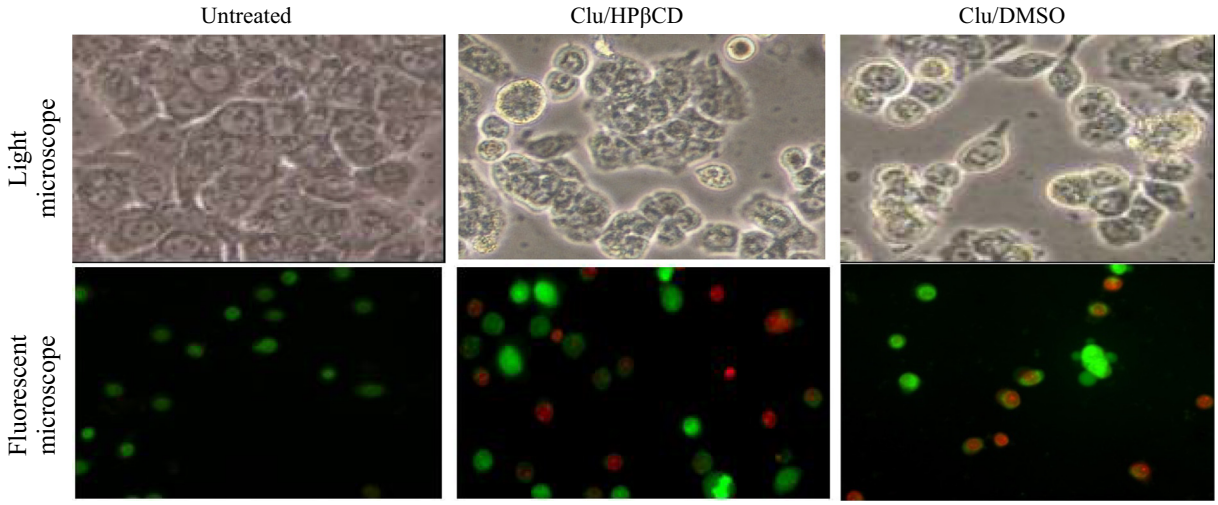

Fig. 7. Morphological alterations in human colon cancer HT29 cell line after treatment with clausenidin complexed with HPβCD or dissolved in DMSO at IC_{50} concentrations, which were calculated through MTT assay. (200×).

brane (red color). However, the cells treated with clausenidin dissolved in the DMSO exhibited more dramatic changes than seen with complexed with HPβCD, at IC_{50} concentrations (Fig. 7).

3.2.3. Caspase-3 and -9

At IC_{50} concentrations, 8.22 μg/mL of clausenidin dissolved in the DMSO possesses highest optical density for caspase-3 (0.3433 3 ± 0.02577) with 3.17-fold increases whilst 2.42 μg/mL of clausenidin incorporated into HPβCD exhibits 1.94-fold increases of optical density (0.21000 ± 0.03115) when a compared to untreated control cells (0.10833 ± 0.01231) (Fig. 8).

The mean optical density for caspase-9 values of the HT29 cancer cells treated with clausenidin, at IC_{50} concentrations, incorporated into HPβCD and dissolved in the DMSO were 0.37933 ± 0. 02938 and 0.54333 ± 0.02368, respectively, which were 351.3% and 503.2% of mean optical density seen with untreated cells (0.1 0798 ± 0.01186), respectively. However, all measurements of caspase-3 and −9 in treated cells are statistically high significant ($P < 0.01$) when compared to control cells (Fig. 8).

3.2.4. Analysis of cell cycle changes and measurement of sub-G_1 DNA content

To investigate whether clausenidin induced cell growth inhibition via alterations in cell cycle distribution, thus, the cell cycle distribution of HT29 cells was analyzed by flow cytometry. The effect of clausenidin, at IC_{50} concentrations, on the cell cycle progression of human colon cancer cell was shown in Fig. 9. The total number of cells in G_0/G_1 decreased slightly from 90.044 ± 3.5937% (for untreated cell) to 88.0328 ± 2.6721%, and 88.2180 ± 1.2630% in the cell treated with the 2.42 μg/mL of clausenidin incorporated into HPβCD, and 8.22 μg/mL of clausenidin dissolved in the DMSO, respectively. The total number of cells in S phases increased significantly ($P < 0.05$) from 4.03762 ± 0.6642% with untreated cells to 4. 46519 ± 0.5307%, after 24 h exposure to 2.42 μg/mL of clausenidin incorporated into HPβCD. On the other hand, the change in number of S phase cells was insignificant ($P > 0.05$) after treatment with 8.22 μg/mL of clausenidin dissolved in the DMSO when compared to untreated cells.

Besides, the total number of cells in M/G_2 phase increased significantly ($P < 0.05$) from 5.91843 ± 0.8641% with untreated cells to 7.50197 ± 0.9652%, and 7.55314 ± 1.0509% after 24 h exposure to IC_{50} concentrations of clausenidin incorporated into HPβCD and clausenidin dissolved in the DMSO, respectively. However, the total number of cells in Sub-G_1 phase increased significantly ($P < 0.05$) from 2.10 ± 0.0593% with untreated cells to 11.17 ± 0.6970% and 11.50 ± 1.1241% after 24 h exposure to IC_{50} concentrations of clausenidin complexed with HPβCD or dissolved in DMSO, respectively, which were 531.9% and 547.6% of measurement seen with untreated cells, respectively (Fig. 9).

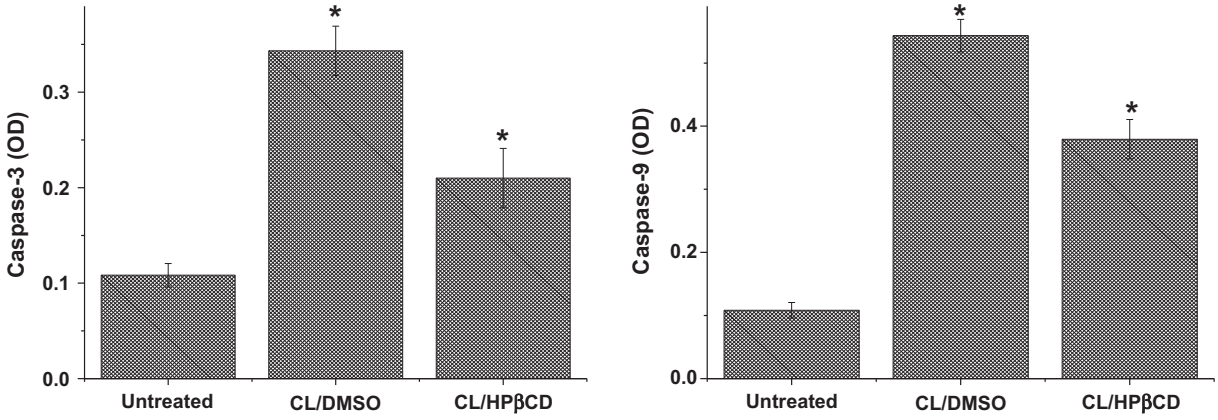

Fig. 8. Caspase-3 and -9 activities of human colon cancer HT29 cell line after treatment with Clausenidin complexed with HPβCD and Clausenidin dissolved in DMSO at IC_{50} concentrations, which were calculated through MTT assay. Mean ± standard deviation (n = 3 wells/treatment). *P < 0.05 compared to non-treated cells.

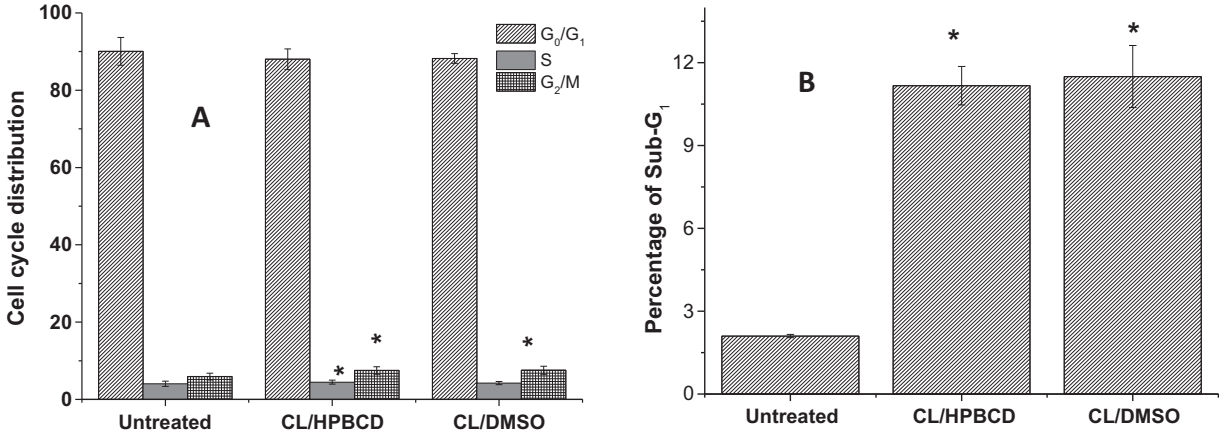

Fig. 9. Effects of clausenidin complexed with HPβCD or dissolved in DMSO at IC_{50} concentrations on cell cycle distribution of HT29 cells and analyzed by flow cytometry. G_0/G_1, G_2/M and S DNA contents indicate the cell phase (A), while and sub-G_1 refers to the proportion of apoptotic cells (B). Values are means ± standard deviations (n = 3 well/treatment). *P < 0.05 compared to non-treated cells.

3.2.5. Reactive oxygen species ROS

At IC_{50} concentrations, 8.22 μg/mL of clausenidin dissolved in the DMSO possesses highest mean ROS levels (65.09 ± 1.20%) with 11.77-fold increases whilst 2.42 μg/mL of clausenidin incorporated into HPβCD exhibits 8.69-fold increases of mean ROS levels (48.06 ± 2.01%) when a compared to untreated colon cancer HT29 cells (5.53 ± 2.50%) (Fig. 10).

4. Discussion

The HPβCD presents the hydrophilic surface and the hydrophobic cavity. The structure of the HPβCD allows the formation of inclusion complex, where our compound with low solubility in water has been included in the cavity of the cyclodextrin and the surface interacts with water. The inclusion complex was formulated to control the dissolution speed of water-low-soluble drug, acting on its prolonged release. It would be ideal to have a more sustained drug delivery system in order to maintain the local drug concentration at a constant level, decreasing side effects, reducing dosing frequency and increasing patient compliance (Al-Qubaisi et al., 2019). Drug release followed the zero-order kinetics. Zero order kinetics refers to the process of constant drug release from a drug delivery system and drug level in the blood remains constant throughout the delivery (Gouda et al., 2017). The zero order model is very suitable to evaluate the kinetic release from the drug delivery device such as oral osmotic tablet, transdermal system, matrix tablet with low soluble drugs and other delivery system (Nagaraju et al., 2009).

The surface morphology of the clausenidin has been changed to irregular particles after complexation with HPβCD. In the work of Al-Qubaisi et al. (2019), it was found that the complexation of thymoquinone of *Nigella sativa* seeds with cyclodextrin caused changes in the morphology of both parent components (Al-Qubaisi et al., 2019).

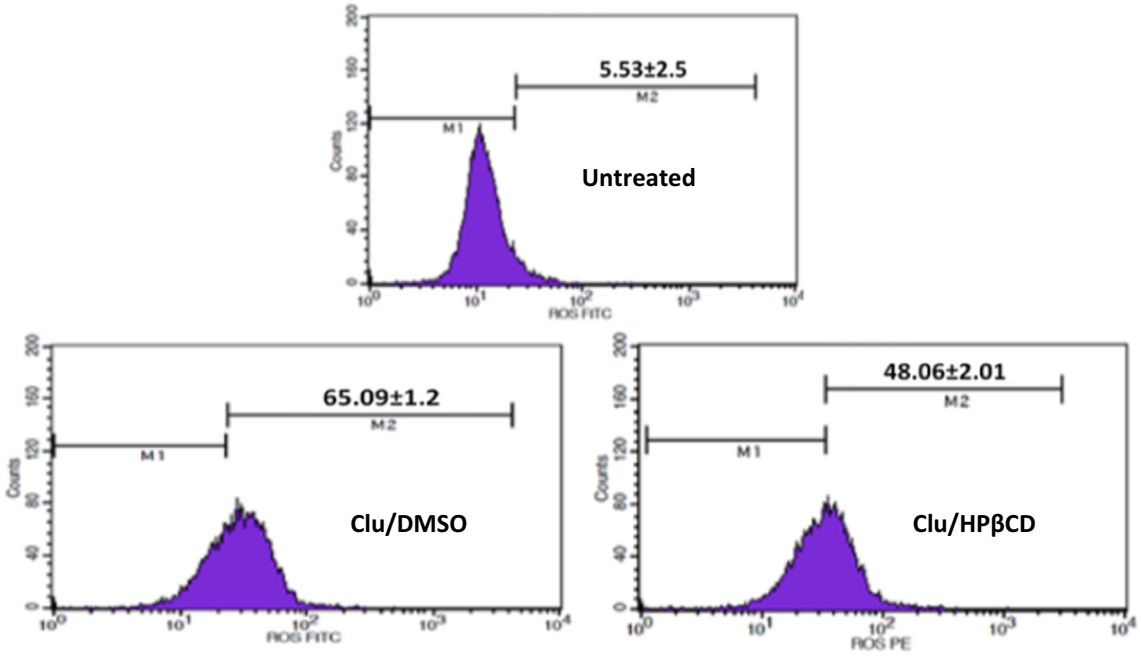

Fig. 10. Percentages of reactive oxygen species in human colon cancer HT29 cell line after treatment with Clausenidin complexed with HPβCD and Clausenidin dissolved in DMSO at IC_{50} concentrations, which were calculated through MTT assay. Mean ± standard deviation (n = 3 wells/treatment).

The DSC curve of inclusion complex shows the total suppression of the event related to the clausenidin, but it also presents the event of the HPβCD related to the loss of water molecules also with deviation to a higher temperature and another endothermic event related to the decomposition. These results indicate that there is an interaction between the clausenidin and the HPβCD. Ashwaq and collaborators (2017) observed the same deviation in the event related to the loss of water molecules from HPβCD, while endothermic peaks of dentatin (which is extracted from *Clausena excavata*) disappeared, in the same way that occurred with the clausenidin (Ashwaq et al., 2017).

The change in the diffraction profile was associated with the formation of complex inclusion with cyclodextrin. XRD result points to successful formation of complex due to disappearance of all peaks belong to clausenidin. Al-Qubaisi et al., (2019) identified the alteration in the diffraction profile after complexation of the thymoquinone compound with HPβCD, indicating the successful formation of the complex inclusion (Al-Qubaisi et al., 2019). This is in good agreement with the DSC results.

The differences presented in FTIR spectra are indicative of the interaction between the clausenidin and the HPβCD, since bands of clausenidin were quite attenuated in formulated inclusion complex. Similar to previous findings (Al-Qubaisi et al., 2019), these observations corroborate the evidence of the formation of an inclusion complex between clausenidin and hydroxypropyl-β-cyclodextrin.

It is well known that the inclusion of the guest molecule inside the cavity of the cyclodextrin cavity induces changes in the chemical shift of the guest protons, and the affected protons of the host (Al-Qubaisi et al., 2019). There were changes in the chemical shifts of HPβCD protons, calculated as the difference in the chemical shift ($\Delta\delta$), in the absence and presence of the clausenidin in the cavity of the cyclodextrin. Consequently, the NMR spectra showed chemical shift changes upon the formation of the inclusion complex complex, a finding similar to that reported earlier (Al-Qubaisi et al., 2019).

To rationalize our experimental results, an *in-silico* method comprising molecular docking was used to judge the stability of the Clu/HPβCD complex. Establishment of H-bonds between host and guest molecules played a key role in stabilizing the inclusion complex. It is evident that molecular docking studies are routinely used to explain the complexation mechanism of host and guest molecules (He et al., 2017; Mady and Aly, 2017; Geng et al., 2019)

When compared to normal colon cells, MTT results quantitatively confirmed the selective targeting effects of complexation with cyclodextrin to introducing higher cellular uptake of encapsulated clausenidin by colon cancer cells. With respect to the HT29 cell line, on the other hand, a much greater cytotoxicity is observed when clausenidin is complexed with the HPβCD than when used alone (IC_{50}: 2.42 μg/mL *vs* 8.22 μg/mL). This might result from the low cellular uptake due to the low solubility of hydrophobic drug in DMSO when a compared to complex as noted by our previous report (AL-Abboodi et al., 2017).

Caspases (intracellular cysteine-aspartic proteases) are the key agents of different types of cell death, including apoptosis, pyroptosis, anoikis, and cornification. Autophagic cell death, necroptosis, and mitotic catastrophe are independent of caspase activity. Caspases are grouped as initiators (caspases 2, 8, 9, and 10) and effectors (caspases 3, 6, and 7) according to their specific function (Al-Qubaisi et al., 2013a, 2013c; Lantto, 2017). The treatment of colon cancer cells with complex inclusion may induce the loss of mitochondrial integrity and, consequently, of the release of cytochrome *c* to the cytosol, which in turn, resulted in activation of caspase-9 stimulating the cascade of caspases, ending in the activation of caspase-3. After 24 h of exposure, the cancer cells showed DNA fragmentation and loss of cell membrane integrity, evidence of cells death from apoptosis and necrosis, respectively as seen under microscope.

Supporting to our published works (Ashwaq et al., 2016; EM Eid et al., 2019), this finding indicated that the inhibitory effect of inclusion complex on cell cycle progression of HT29 cells was mainly due to apoptosis induction and M/G_2 arrest.

Additionally, Clu/HPβCD inclusion complex induces the activation of apoptosis through a signaling pathway dependent on the production of reactive oxygen species The oxidation of NADH initiates the electron flow in the mitochondrial electron transport chain leading to the decrease of O_2 to water and the production of ATP. However, a small percentage of the O_2 does not get fully reduced due to leakage of electrons from complexes 1 and 3 in the electron transport chain (Allison and Scheffler, 2009). These reactive oxygen species can cause damage, especially to macromolecules (DNA, proteins, and lipids) and also to mitochondria resulting in more mitochondrial dysfunction and increased production of reactive oxygen species (Kadenbach, 2012).

5. Conclusion

The characterization of our inclusion complex led to conclusive results on the way in which the interaction of clausenidin and HPβCD occurs. Our inclusion complex have improved the ability to selectively deliver of clausenidin to target colon cancer cells with almost no cytotoxicity to normal colon cells, as well as increased its solubility. Although progress has been made towards a drug delivery system for clausenidin and its *in vitro* anticancer, the work is not completed. *In vivo* studies can be performed to build on the successes achieved in this current work, in order to help improve the drug delivery system.

References

AL-Abboodi, A.S., Rasedee, A., Abdul, A.B., Taufiq-Yap, Y.H., Alkaby, W.A.A., Ghaji, M. S., Waziri, P.M., Al-Qubaisi, M.S., 2017. Anticancer effect of dentatin and dentatin-hydroxypropyl-β-cyclodextrin complex on human colon cancer (HT-29) cell line. Drug Des. Develop. Thera. 11, 3309.

Al-Qubaisi, M., Rosli, R., Subramani, T., Omar, A.R., Yeap, S.K., Ali, A.M., Alitheen, N.B., 2013a. Goniothalamin selectively induces apoptosis on human hepatoblastoma cells through caspase-3 activation. Nat. Prod. Res. 27, 2216–2218.

Al-Qubaisi, M.S., Rasedee, A., Flaifel, M.H., Ahmad, S.H., Hussein-Al-Ali, S., Hussein, M.Z., Eid, E.E., Zainal, Z., Saeed, M., Ilowefah, M., 2013b. Cytotoxicity of nickel zinc ferrite nanoparticles on cancer cells of epithelial origin. Int. J. Nanomed. 8, 2497.

Al-Qubaisi, M.S., Rasedee, A., Flaifel, M.H., Ahmad, S.H., Hussein-Al-Ali, S., Hussein, M.Z., Zainal, Z., Alhassan, F.H., Taufiq-Yap, Y.H., Eid, E.E., 2013c. Induction of apoptosis in cancer cells by NiZn ferrite nanoparticles through mitochondrial cytochrome C release. Int. J. Nanomed. 8, 4115.

Al-Qubaisi, M.S., Rasedee, A., Flaifel, M.H., Eid, E.E., Hussein-Al-Ali, S., Alhassan, F.H., Salih, A.M., Hussein, M.Z., Zainal, Z., Sani, D., 2019. Characterization of thymoquinone/hydroxypropyl-β-cyclodextrin inclusion complex: application to anti-allergy properties. Eur. J. Pharm. Sci. 133, 167–182.

Allison, W.S., Scheffler, I., 2009. Mitochondrial Function, Part A: Mitochondrial Electron Transport Complexes and Reactive Oxygen Species. Elsevier Science.

Arbab, I.A., Abdul, A.B., Aspollah, M., Abdullah, R., Abdelwahab, S.I., Mohan, S., Abdelmageed, A., 2011. Clausena excavata Burm. f. (Rutaceae): a review of its traditional uses, pharmacological and phytochemical properties. J. Med. Plants Res. 5, 7177–7184.

Arcangelo, V.P., Peterson, A.M., 2006. Pharmacotherapeutics for Advanced Practice: A Practical Approach. Lippincott Williams & Wilkins.

Ashwaq, A.-A.S., Al-Qubaisi, M.S., Rasedee, A., Abdul, A.B., Taufiq-Yap, Y.H., Yeap, S. K., 2016. Inducing G2/M cell cycle arrest and apoptosis through generation reactive oxygen species (ROS)-mediated mitochondria pathway in HT-29 cells by dentatin (DEN) and dentatin incorporated in hydroxypropyl-β-cyclodextrin (DEN-HPβCD). Int. J. Mol. Sci. 17, 1653.

Ashwaq, A.-A.S., Rasedee, A., Abdul, A.B., Taufiq-Yap, Y.H., Al-Qubaisi, M.S., Eid, E.E., 2017. Characterization, drug release profile and cytotoxicity of Dentatin-Hydroxypropyl-β-Cyclodextrin complex. J. Incl. Phenom. Macrocycl. Chem. 87, 167–178.

Bourgaud, F., Poutaraud, A., Guckert, A., 1994. Extraction of coumarins from plant material (Leguminosae). Phytochem. Anal. 5, 127–132.

Brezani, V., Smejkal, K., Hosek, J., Tomasova, V., 2018. Anti-inflammatory natural prenylated phenolic compounds-potential lead substances. Curr. Med. Chem. 25, 1094–1159.

Cao, Z., Li, W., Liu, R., Li, X., Li, H., Liu, L., Chen, Y., Lv, C., Liu, Y., 2019. pH-and enzyme-triggered drug release as an important process in the design of anti-tumor drug delivery systems. Biomed. Pharmacother. 118, 109340.

Clausse, D., Dumas, J.P., 2016. Supercooling, Crystallization and Melting within Emulsions and Divided Systems: Mass, Heat Transfers and Stability. Bentham Science Publishers.

Damsud, T., Chanwun, T., Kaewpiboon, C., 2017. Antidiabetic agents with α-glucosidase inhibition and antioxidant capacity from the shoots of Clausena cambodiana Guill. Int J Agric Technol 13, 449–456.

Earnest, C.M., Measurements, A.C.E.-o.T., 1988. Compositional Analysis by Thermogravimetry. ASTM.

EM Eid, E., S Alanazi, A., Koosha, S., A Alrasheedy, A., Azam, F., M Taban, I., Khalilullah, H., Sadiq Al-Qubaisi, M., Alshawsh, M., 2019. Zerumbone induces apoptosis in breast cancer cells by targeting αvβ3 integrin upon co-administration with TP5-iRGD peptide. Molecules 24, 2554.

Florence, A.T., Salole, E.G., 2013. Routes of Drug Administration: Topics in Pharmacy. Elsevier Science.

Geng, Q., Li, T., Wang, X., Chu, W., Cai, M., Xie, J., Ni, H., 2019. The mechanism of bensulfuron-methyl complexation with β-cyclodextrin and 2-hydroxypropyl-β-cyclodextrin and effect on soil adsorption and bio-activity. Sci. Rep. 9, 1–11.

Gouda, R., Baishya, H., Qing, Z., 2017. Application of mathematical models in drug release kinetics of carbidopa and levodopa ER tablets. J. Dev Drugs 6.

Gratieri, T., Pinho, L.A., Oliveira, M.A., Sa-Barreto, L.L., Marreto, R.N., Silva, I.C., Gelfuso, G.M., Quintans, J.d.S.S., Quintans-Junior, L.J., Cunha-Filho, M., 2020. Hydroxypropyl-β-cyclodextrin-complexed naringenin by solvent change precipitation for improving anti-inflammatory effect in vivo. Carbohydrate Polym. 231.

He, J., Zheng, Z.-P., Zhu, Q., Guo, F., Chen, J., 2017. Encapsulation mechanism of oxyresveratrol by β-cyclodextrin and hydroxypropyl-β-cyclodextrin and computational analysis. Molecules 22, 1801.

Joshi, B., Kamat, V., Saksena, A., 1967. Structures of clausenin and clausenidin two new pyranocoumarins from the roots of clausena heptaphylla Wt. & Arn. Tetrahedron 23, 4785–4789.

Kadenbach, B., 2012. Mitochondrial Oxidative Phosphorylation: Nuclear-Encoded Genes, Enzyme Regulation, and Pathophysiology. Springer, New York.

Kongkathip, B., Kongkathip, N., Sunthitikawinsakul, A., Napaswat, C., Yoosook, C., 2005. Anti-HIV-1 constituents from Clausena excavata: Part II. carbazoles and a pyranocoumarin. Phytotherapy Res.: Int. J. Devoted Pharmacol. Toxicol. Evaluat. Natl. Prod. Derivat. 19, 728–731.

LaManna, J.C., Puchowicz, M.A., Xu, K., Harrison, D.K., Bruley, D.F., 2011. Oxygen Transport to Tissue XXXII. Springer, US.

Lantto, T.A., 2017. Cytotoxic and apoptotic effects of selected phenolic compounds and extracts from edible plants.

Mady, F.M., Aly, U.F., 2017. Experimental, molecular docking investigations and bioavailability study on the inclusion complexes of finasteride and cyclodextrins. Drug Des. Develop. Therapy 11, 1681.

Mendyk, A., Jachowicz, R., Fijorek, K., Dorozynski, P., Kulinowski, P., Polak, S., 2012. KinetDS: an open source software for dissolution test data analysis. Dissolut. Technol. 19, 6–11.

Nagaraju, R., Meera, D.S., Kaza, R., Arvind, V.V., Venkateswarlu, V., 2009. Core-in-cup tablet design of metoprolol succinate and its evaluation for controlled release. Curr. Drug Discov. Technol. 6, 299–305.

Nicol, T.W., Matubayasi, N., Shimizu, S., 2016. Origin of non-linearity in phase solubility: solubilisation by cyclodextrin beyond stoichiometric complexation. PCCP 18, 15205–15217.

Patel, N., Chotai, N., Patel, J., Soni, T., Desai, J., Patel, R., 2008. Comparison of in vitro dissolution profiles of oxcarbazepine-HP b-CD tablet formulations with marketed oxcarbazepine tablets. Dissolut. Technol. 15, 28–34.

Praphanwittaya, P., Saokham, P., Jansook, P., Loftsson, T., 2020. Aqueous solubility of kinase inhibitors: II the effect of hexadimethrine bromide on the dovitinib/γ-cyclodextrin complexation. J. Drug Deliv. Technol. 55, 101463.

Ramawat, K.G., Mérillon, J.-M., 2013. Natural Products: Phytochemistry, Botany and Metabolism of Alkaloids, Phenolics and Terpenes. Springer.

Saokham, P., Muankaew, C., Jansook, P., Loftsson, T., 2018. Solubility of cyclodextrins and drug/cyclodextrin complexes. Molecules 23, 1161.

Srivastava, P., Pandey, A., 2015. Natural products and derivatives: biological and pharmacological activities. Biochem. Cellular Arch. Muzaffarna 1, 1–38.

Su, C.-R., Yeh, S.F., Liu, C.M., Damu, A.G., Kuo, T.-H., Chiang, P.-C., Bastow, K.F., Lee, K.-H., Wu, T.-S., 2009. Anti-HBV and cytotoxic activities of pyranocoumarin derivatives. Bioorg. Med. Chem. 17, 6137–6143.

Sunthitikawinsakul, A., Kongkathip, N., Kongkathip, B., Phonnakhu, S., Daly, J.W., Spande, T.F., Nimit, Y., Rochanaruangrai, S., 2003. Coumarins and carbazoles from Clausena excavata exhibited antimycobacterial and antifungal activities. Planta Med. 69, 155–157.

Trott, O., Olson, A.J., 2010. AutoDock Vina: improving the speed and accuracy of docking with a new scoring function, efficient optimization, and multithreading. J. Comput. Chem. 31, 455–461.

Waziri, P.M., Abdullah, R., Rosli, R., Omar, A.R., Abdul, A.B., Kassim, N.K., Malami, I., Etti, I.C., Sani, J.A.M., Lila, M.A.M., 2018. Clausenidin induces caspase 8-dependent apoptosis and suppresses production of VEGF in liver cancer cells. Asian Pacific J. Cancer Prevent.: APJCP 19, 917.

Waziri, P.M., Abdullah, R., Yeap, S.K., Omar, A.R., Abdul, A.B., Kassim, N.K., Malami, I., Karunakaran, T., Imam, M.U., 2016. Clausenidin from Clausena excavata induces apoptosis in hepG2 cells via the mitochondrial pathway. J. Ethnopharmacol. 194, 549–558.